Research Article | Vol. 12, No. 8 / 1 August 2021 / Biomedical Optics Express 4795
Biomedical Optics EXPRESS

High-performance surface-enhanced Raman spectroscopy chip integrated with a micro-optical system for the rapid detection of creatinine in serum

FENG YANG,[1,2] PING WEN,[1,2] GANG LI,[1] ZHISEN ZHANG,[3] CHUANG GE,[4] AND LI CHEN[1,*]

[1]College of Optoelectronic Engineering, Key Laboratory of Optoelectronic Technology and Systems, Ministry of Education, Key Disciplines Lab of Novel Micro-Nano Devices and System Technology, Chongqing University, Chongqing 400044, China
[2]School of Intelligent Manufacturing, Sichuan University of Arts and Science, Dazhou 635000, China
[3]School of Intelligent Manufacturing, Panzhihua University, Panzhihua 617000, China
[4]Key Laboratory of Translational Research for Cancer Metastasis and Individualized Treatment, Chongqing University Cancer Hospital, Chongqing 400030, China
*cl2009@cqu.edu.cn

Abstract: To improve the sensitivity of disease biomarker detection, we proposed a high-performance surface-enhanced Raman spectroscopy (SERS) chip integrated with a micro-optical system (MOS). The MOS, which is based on the micro-reflecting cavity and the micro-lens, optimizes the optical matching characteristics of the SERS substrate and the Raman detection system, and greatly improves the SERS detection sensitivity by improving the collection efficiency of the Raman scattering signal. A uniform single layer of silver nanoparticles on a gold film was prepared as the SERS substrate using a liquid-liquid interface self-assembly method. The micro-reflecting cavity and micro-lens were prepared using micro-processing technology. The SERS chip was constructed based on the MOS and the Au film-based SERS substrate, and experimental results showed an EF of 1.46×10^8, which is about 22.4 times higher than that of the Si-based SERS substrate. The chip was used for the detection of creatinine and the detection limit of creatinine in aqueous solution was 1 μM while the detection limit in serum was 5 μM. In addition, SERS testing was conducted on serum samples from normal people and patients with chronic renal impairment. Principal component analysis and linear discriminant analysis were used for modeling and identification, and the results showed a 90% accuracy of blind sample detection. These results demonstrate the value of this SERS chip for both research and practical applications in the fields of disease diagnosis and screening.

1. Introduction

Serum creatinine is a key biomarker for the diagnosis and monitoring of kidney disease [1–3]. Rapid and sensitive creatinine detection is thus important. Surface-enhanced Raman spectroscopy (SERS) technology has many advantages such as immunity to water interference, "fingerprint" information, and rapid and non-destructive detection [4–9], and has great potential for the rapid detection of disease biomarkers [10–16]. For example, Stosch et al. used isotope labeling for quantitative SERS detection of creatinine in serum [17]. In biological samples, due to factors such as complex sample composition and weak Raman scattering, the key to achieving accurate detection is to obtain a sufficiently high detection sensitivity. Moreover, in order to avoid the sample being damaged by high temperature, the excitation power is often limited. Therefore, there are two main strategies to improve SERS detection sensitivity: one is to optimize the

#434053 https://doi.org/10.1364/BOE.434053
Journal © 2021 Received 11 Jun 2021; revised 5 Jul 2021; accepted 6 Jul 2021; published 12 Jul 2021

Biomedical Optics EXPRESS

plasmonic nanostructure, and the other is to improve the collection efficiency of the Raman scattering signals.

In the preparation of plasmonic nanostructures, various methods have been developed to prepare SERS substrates with ultra-high sensitivity [18–21]. According to the SERS electromagnetic enhancement mechanism [22], the Raman enhancement efficiency is extremely sensitive to the size of the nanogap. Therefore, the key to preparing SERS substrates is the construction and optimization of the nano-gap. Plasmonic nano-pattern arrays with nano-gaps can be prepared using advanced micro-nano manufacturing technologies, such as electron-beam lithography (EBL) [23–25], focused ion beam (FIB) [26,27], and nanoimprint lithography (NIL) [28,29]. However, such methods often require sophisticated equipment and complex operations. Chemical synthesis methods are widely used in SERS applications due to their simplicity and convenience. A simple reduction reaction can be used to prepare gold/silver nanoparticles [30,31], and assemble them into a uniformly distributed nanoparticle array to obtain a highly active SERS substrate [32,33].

Improving the collection efficiency of Raman signals is another important strategy to improve the sensitivity of SERS detection. According to the principle of Raman scattering, the Raman signal generated by the molecule will scatter randomly in all directions. Only the signals that enter the aperture angle of the objective lens will be collected, and the signals outside the aperture angle will be wasted. Most research on SERS has used commercial Raman microscopes to collect Raman spectra, often only by using a larger numerical aperture objective to improve the signal collection efficiency to obtain higher detection sensitivity. By designing precious optical antenna [34] (such as two-dimensional gratings) or adopting prism-type surface plasmon structures [35–37], the SERS signal can be directionally radiated, and the excitation and collection optical paths at specific angles can achieve higher signal collection efficiency. However, this method often requires the additional design of a complex optical path system. For example, Xu's research group designed a special aplanatic solid immersion lens and developed a spectrometer called iPERS [37], which used excitation evanescent wave excitation and reverse collection to achieve the directional emission of SERS signals, thereby improving SERS signal collection efficiency.

Here, we designed and prepared a high-performance SERS chip integrated with a micro-optical system (MOS). The MOS functioned to optimize the optical matching between the SERS substrate and the Raman detection system to improve the collection efficiency of the SERS signal, thereby effectively improving the detection sensitivity. First, a single uniform layer of silver nanoparticles was prepared by the liquid-liquid interface self-assembly method, which was used as the SERS active substrate to guarantee reliable Raman detection. Based on our previous research [38], we designed the MOS to improve the SERS detection sensitivity and conducted verification experiments. The prepared SERS chip was used to investigate creatinine detection in both aqueous and serum solutions, and the detection limit of creatinine in aqueous solution and serum was 1 μM and 5 μM, respectively, demonstrating the feasibility of SERS detection of serum creatinine. In addition, SERS tests were performed on serum samples from normal people and patients with chronic renal failure. Using principal component analysis and the linear discriminant method to model and identify the serum SERS spectra in renal patients and controls, the accuracy of the blind sample detection reached 90%. The SERS chip thus exhibits feasible potential application for the rapid detection of early disease biomarkers.

2. Experiments and methods

2.1. Synthesis of silver nanoparticles and assembly of monolayer particle films

Silver nanoparticles were prepared according to the method of Lee and Meisel [30]. The specific preparation process is provided in the supporting material. As shown in Figure S1, except for a small number of rod-shaped silver nanoparticles, most of the prepared silver nanoparticles were spherical. The characterization results showed that the average particle size of silver nanoparticles

Biomedical Optics EXPRESS

was about 49.3 nm. Before use, the silver nanosol was centrifuged at 8000 rpm for 5 minutes, the supernatant removed, and the precipitate ultrasonically dispersed in deionized water.

We used the liquid-liquid interface assembly method to assemble a single layer of silver nanoparticles as the SERS substrate. The specific process is provided in the supporting material (Figure S2 and Figure S3).

2.2. Preparation of the SERS chip

The SERS chip was essentially composed of a SERS substrate, an inverted pyramid structure micro-reflecting cavity, and a micro-lens. The flowchart of the manufacturing process is shown in Fig. 1.

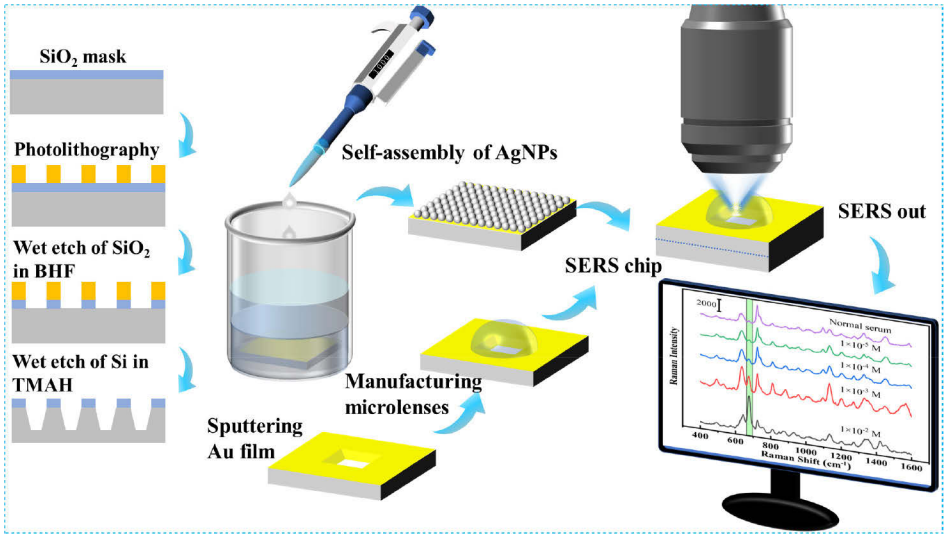

Fig. 1. Schematic diagram showing preparation of the SERS chip.

According to the method established in our previous research [38], a micro-reflective cavity with an inverted pyramid through-hole structure based on a <100> crystal orientation Si wafer was prepared. Briefly, the photoresist was spin-coated on the surface of the Si oxide wafer, and the exposed Si dioxide was removed by photolithography and buffered hydrofluoric acid (BHF). After removing the photoresist with acetone, a regular square pattern was formed on the surface of the Si oxide wafer. Anisotropic wet etching with tetramethyl ammonium hydroxide (TMAH, 12.5% wt) solution was performed at 90°C until formation of the through-holes of the inverted pyramid structure. Then, a smooth Au film (120 nm thickness) was sputtered on its surface by magnetron sputtering technology to form the micro-reflective cavity.

The micro-reflective cavity was filled with a mixture of PDMS prepolymer and curing agent (mixed at a mass ratio of 10:1), degassed in a vacuum box for 30 minutes, and cured at 90°C for 60 minutes. SU-8 photoresist (0.4μL) was used to cover the top of the inverted pyramid in the shape of a spherical crown, which was then exposed under violet light for about 1 minute to form the micro-lens after curing. The micro-lens and the micro-reflection cavity together constitute the micro-optical system. Finally, it was bonded to the SERS substrate to form the SERS chip. The photographic picture of the prepared SERS chip is shown in Fig. S4.

2.3. Simulation analysis

The electric field distribution of the nanoparticles was simulated by the wave optics module of COMSOL Multiphysics 5.4 software. The geometric model consisted of a flat substrate and

Biomedical Optics EXPRESS

a dimer of silver nanoparticles. The particle size of the silver nanoparticles was set to 50 nm, which is essentially the same as the average particle size of the silver nanoparticles prepared in this experiment. The gaps between the nanoparticles and the substrate and adjacent nanoparticles were set to 2 nm. Incident light (785 nm) with X-direction polarization was propagated in the -Z direction.

The Raman signal collection performance of the MOS was simulated and analyzed by the ray optics module of COMSOL Multiphysics 5.4. The geometric model included an inverted pyramid structure reflecting cavity, a plano-convex lens, and a "mirror" representing the collection objective. It was assumed that the Raman scattering signals are uniformly emitted in all directions upward from the center of the bottom surface of the micro-reflecting cavity, and that all the Raman scattering signals had the same power. Under the combined action of the micro-reflecting cavity and the micro-lens, the Raman signal originally outside the numerical aperture was collected. The incident heat flux of the "mirror" was calculated to characterize the Raman scattering signal collection efficiency of the MOS.

2.4. Performance characterization of the MOS

The internal structure of monocrystalline Si is regular and stable, and its Raman signal fluctuates little. Therefore, we chose a single crystal Si wafer as the Raman probe to characterize the performance of the MOS. We attached the MOS to the monocrystalline Si wafer and then directly collected the Raman signal of the monocrystalline Si from the 3D structure. The Raman test conditions were set as follows: laser wavelength 785 nm, laser power 34.8 mW, and integration time 3 s.

At the same time, we collected the R6G Raman signal in the SERS chip and compared it with the R6G Raman intensity collected on the planar SERS substrate under the same test conditions to further verify the SERS signal collection efficiency of the MOS. The Raman test conditions were set as follows: laser wavelength 785 nm, laser power 5 mW, and integration time 1 s.

2.5. SERS detection of creatinine

Creatinine powder (99%, 114.26 mg) was weighed out and dissolved in 10 ml of deionized water to obtain a 1×10^{-1} M aqueous creatinine solution. This solution was then serially diluted with deionized water to prepare a series of creatinine solutions. Serum samples from patients with chronic renal impairment (serum creatinine concentration greater than 100 μM) and normal people were collected from the Chongqing University Cancer Hospital and stored in a freezer at -20°C before use. Serum creatinine solutions of different concentrations (1×10^{-2} M to 1×10^{-5} M) were prepared by mixing 2×10^{-2} M to 2×10^{-5} M creatinine aqueous solution with healthy human serum in equal proportions. Deionized water and serum mixed in a 1:1 ratio were used as the controls. Drop 2 microliters of sample on the SERS substrate, cover the micro-optical system plate, and keep the two closely attached, and then collect the SERS spectrum.

3. Results and discussion

3.1. Preparation and characterization of the silver nanoparticle film

Figures 2(a) and 2(b) show the silver nanoparticle films prepared on the surface of the Si wafer and Au-plated Si wafer, respectively, by the liquid-liquid interface self-assembly method. It can be seen from the figures that the silver nanoparticles on the two substrates are both uniformly distributed in a single layer except for a small amount of accumulation and blank, which provides a guarantee for reliable Raman enhancement.

To compare the effects of different substrates on the Raman enhancement, we collected SERS spectra of R6G (10^{-8} M) under the same test conditions. To make the detection result more reliable, six random points were selected to collect the spectrum and were averaged

Biomedical Optics EXPRESS

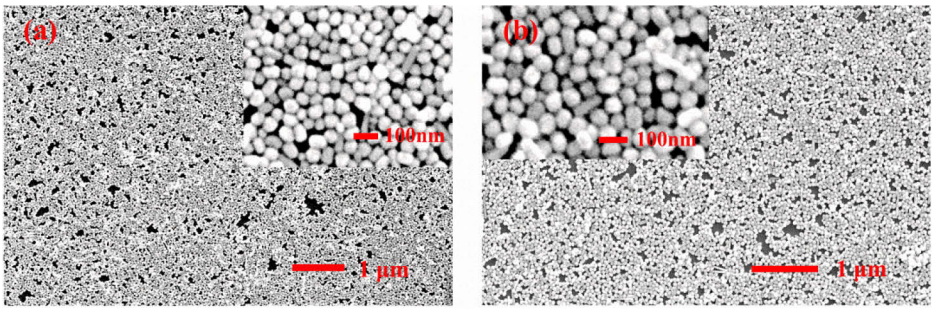

Fig. 2. SEM pictures of single-layer silver nanoparticle film on the (a) Si wafer and (b) Au -plated Si wafer.

as the final detection result. It can be seen from Fig. 3(a) that the SERS intensity collected on the Au film-based SERS substrate is significantly higher than that on the Si wafer-based SERS substrate. The calculated results of the analytical enhancement factor (AEF) for the Si wafer-based SERS substrate and the Au film-based SERS substrate were $AEF_{Si\ wafer}=6.23\times10^6$ and $AEF_{Au\ film}=3.51\times10^7$ respectively, and the detailed calculation process is shown in Figure S5. The calculated results showed that the AEF of the Au film-based SERS substrate was about 5.63 times that of the Si wafer-based SERS substrate. The primary reason for this is that there was plasmonic coupling between the Au film and the silver nanoparticles [19,39], which increases the electric field strength of the "hot spots" in the gaps between the nanoparticles, thereby increasing the SERS intensity. Subsequent SERS experiments were performed using the single-layer silver nanoparticles film on an Au-plated Si wafer.

Figures 3(c) and 3(d) show the simulation results of the electric field distribution of the silver nanoparticle dimer placed on the Si wafer and the Au film, respectively. According to the electric field enhancement theory of SERS [22], it was calculated that the enhancement factor of the silver nanoparticle dimer on the Au film was about 9 times that of the Si wafer. We infer that the possible reasons for the difference between the simulation analysis and the experimental results are: 1) The simplified model was used in the simulation, which is different from the actual situation; 2) The "hot spot" with the largest electric field strength was used to calculate the enhancement factor in the simulation while the experiments gave only the average enhancement factor.

Signal uniformity is an important parameter in the evaluation of the performance of SERS substrates. We used R6G as the Raman probe molecule to perform the SERS mapping test in an area of 30×26 μm^2 on the Au-plated Si SERS substrate. The scanning steps on both the x- and y-axes directions were set to 2 μm, and a total of 224 sets of SERS spectra were collected. Figure 3(b) shows the SERS mapping images of R6G at 612, 1358, and 1509 cm^{-1}, and the relative standard deviations (RSD) of the SERS peaks at 612, 1358, and 1509 cm^{-1} were calculated to be 10.7%, 9.3%, and 11.2%, respectively.

3.2. Preparation and performance characterization analysis of the micro-optical system

Figures 4(a) and 4(b) show the top and side SEM images, respectively, of the micro-reflective cavity prepared by the wet etching method. It can be seen that it appears as a typical inverted pyramid structure. The measured angle between the sidewall and the bottom surface was 54.7°, which is consistent with the theoretical result of the angle between the (111) plane and the (100) plane of monocrystalline Si. Figure 4(c) is an electron micrograph of the micro-lens covering the micro-reflecting cavity. The diameter of the micro-lens measured under the microscope

Biomedical Optics EXPRESS

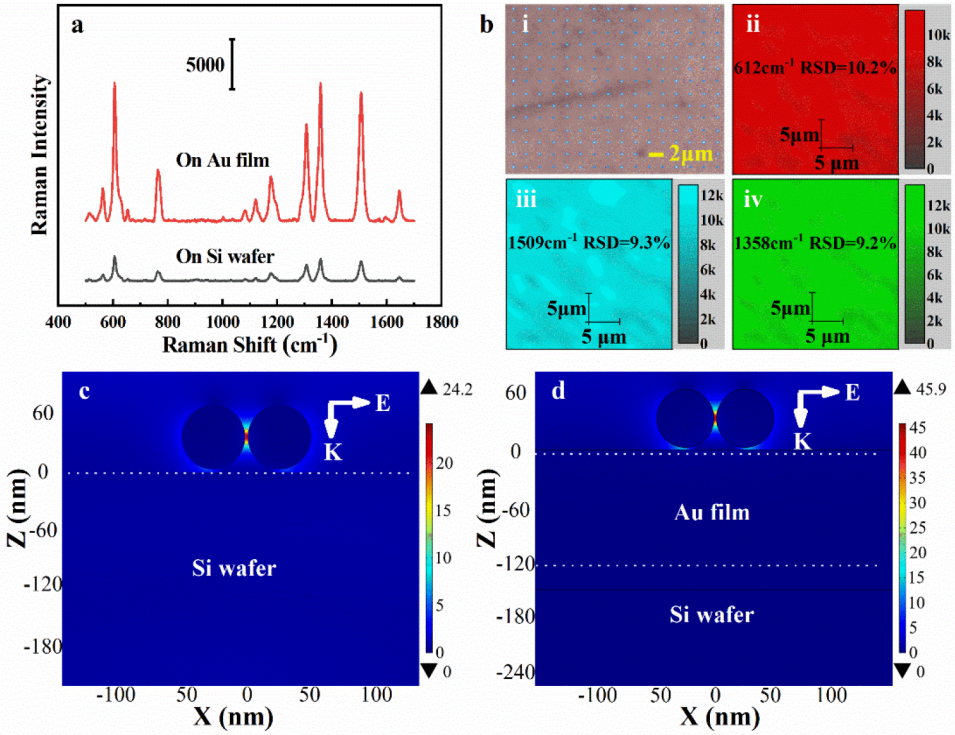

Fig. 3. (a) SERS spectra of R6G collected from the single-layer silver nanoparticle film on (i) Au film and (ii) Si wafer. (b) SERS mapping of R6G (10^{-8} M) on the Au film-based SERS substrate, (i) Optical image of the region for Raman mapping, (ii-iv) Raman maps targeting the R6G signal at 612, 1511, and 1363 cm^{-1}, respectively. Simulation results of the electric field distribution of the dimer of silver nanoparticles on the (c) Au film and the (d) Si wafer.

was about 1061.7 microns, and Fig. 4(d) is the measurement result of the contact angle of the micro-lens.

Figure 5(a) shows the Raman spectra test results of the monocrystalline Si with and without using the MOS. The calculated result based on the peak value of 520 cm^{-1} showed that the Raman intensity collected in the MOS was approximately 4.16 times that of the direct measurement on the Si wafer. This is due to the improved collection efficiency of Raman scattered signals by the MOS.

Figures 5(b) and 5(c) present the simulation results of the optical power density distribution on the collecting surface with and without the use of the MOS, respectively. It can be seen that when using the MOS, most of the light energy was distributed in the center of the collecting surface, which is more helpful for the objective lens to the collection of Raman scattering signals. Figure 5(d) shows the total light energy on the collecting surface in the two cases. Calculations showed that when the MOS is used, the total light energy is approximately 4.31 times that when MOS is not used, which is consistent with the experimental results.

Furthermore, we used the flat SERS substrate (Au film-based SERS substrate) and the SERS chip (Au film-based SERS substrate+ MOS) to collect the R6G (10^{-8}M) SERS spectra under the same test conditions. As shown in Fig. 5(e), the Raman intensity collected in the SERS chip was significantly stronger than the Raman intensity on the flat SERS substrate. The calculated peak value at 1358 cm^{-1} showed that the Raman intensity collected on the SERS chip was

Biomedical Optics EXPRESS

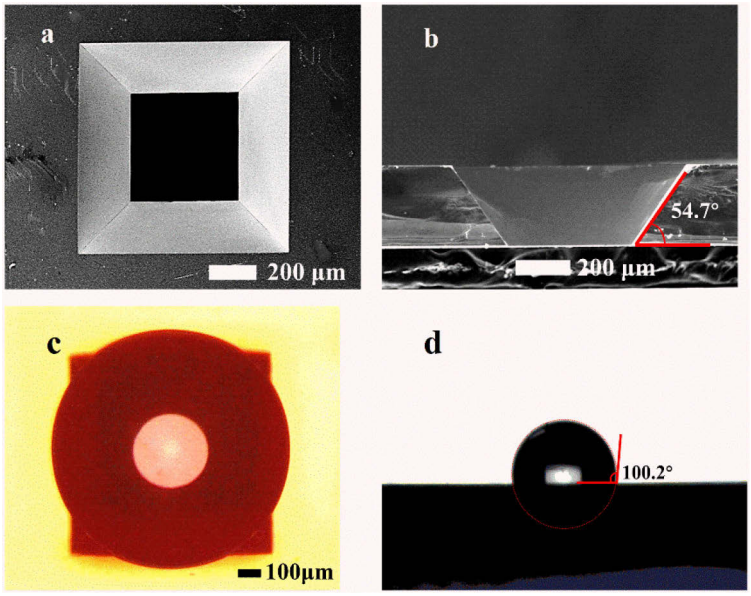

Fig. 4. (a) SEM image of the micro-reflective cavity. (b) Side view of the micro-reflective cavity. (c) Electron micrograph of the micro-lens. (d) Contact angle measurement of the micro-lens.

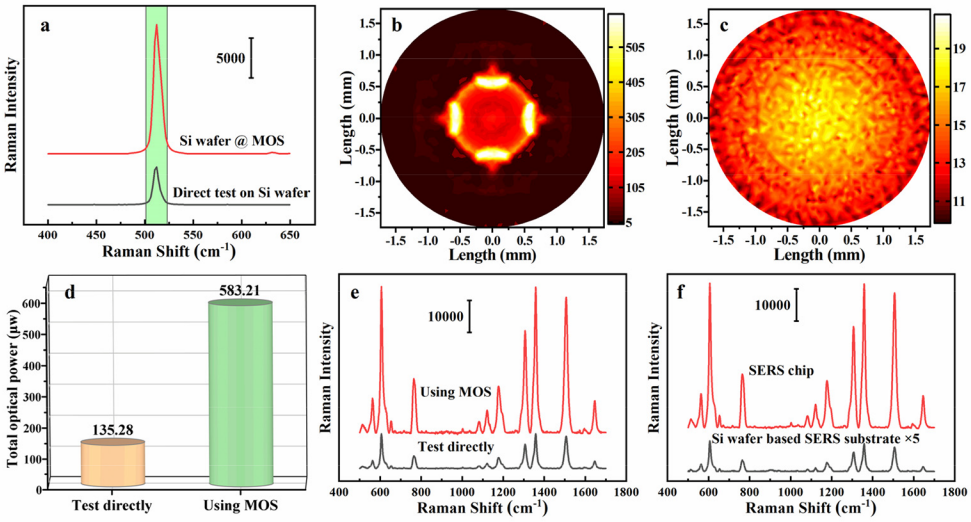

Fig. 5. (a) Raman spectra of monocrystalline Si with and without using the MOS. Simulation results of the optical power density distribution on the collecting surface when using MOS (b) and without using MOS (c). (d) Comparison of ray optical simulation results. (e) Raman spectra of R6G collected on the Au film-based SERS substrates with and without integrated the MOS. (f) Raman spectra of R6G collected on the SERS chip and the Si wafer-based SERS substrate.

Biomedical Optics EXPRESS

about 4.15 times that on the flat SERS substrate, which was consistent with the above-mentioned experimental and simulation results. The experimental results further verified the correctness of the design scheme. Using the same calculation method described in Section 3.1, the AEF of the SERS chip was as high as 1.46×10^8. It can be seen that the MOS can greatly increase the SERS signal strength, thereby improving the Raman detection sensitivity. Figure 5(f) shows the comparison of the R6G Raman spectra collected using the SERS chip and the Si-based SERS substrate. The calculation results show that the AEF of the SERS chip was about 22.4 times higher than that of the Si-based SERS substrate.

3.3. Creatinine detection using the SERS chip

3.3.1. Creatinine aqueous solution detection

We used the prepared SERS chip to perform SERS creatinine detection in aqueous solutions with different creatinine concentrations. The Raman test conditions were: laser wavelength 785 nm, laser power 7.8 mW, and integration time 3 seconds. For each concentration, a total of 6 SERS spectra were collected at different random points and then averaged as the final result. As shown in Fig. 6(a), the characteristic creatinine peak of creatinine at 678 cm^{-1} could be clearly seen from the SERS spectra. The Raman peak at 678 cm^{-1} is the result of shear vibration of the ring plane, stretching vibration of the C-NH_2 moiety, the ring, and C-O [14,40]. It can be seen from the figure that, as the concentration of creatinine decreased, the intensity of the 678 cm^{-1} peak decreased significantly. When the concentration was reduced to 1×10^{-6} M, the creatinine Raman peak could still be clearly distinguished (Fig. 6(a)). This shows that the detection limit of creatinine by the SERS chip was as low as 1×10^{-6} M.

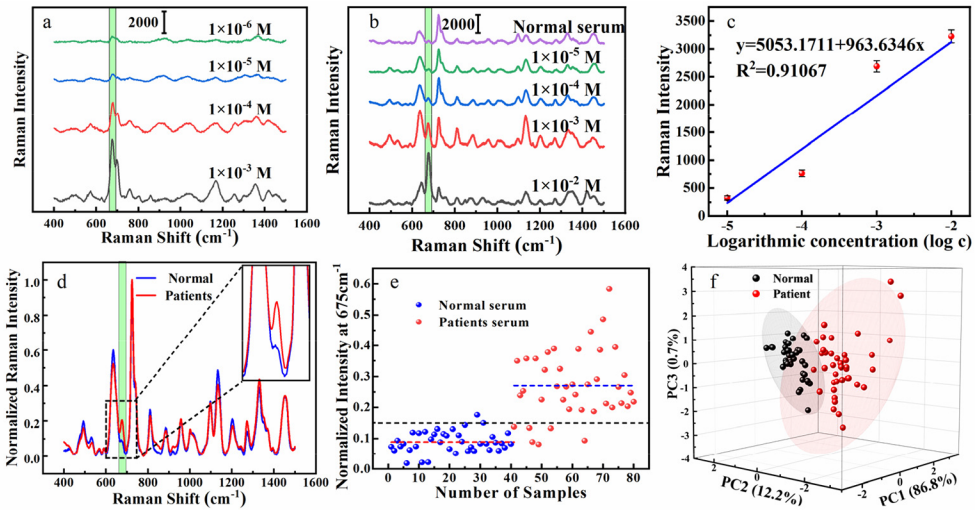

Fig. 6. (a) SERS spectra of creatinine aqueous solutions of different concentrations. (b) SERS spectra of normal serum with different concentrations of creatinine. (c) Fitting curve of the peak intensity at 678 cm^{-1} and logarithmic concentration. (d) Normalized SERS spectra of normal and patient serum. (e) The peak distribution at 678 cm^{-1} of normalized SERS spectra of normal and patient serum. (f) SERS spectral model training set of normal and patient serum.

3.3.2. SERS detection of serum creatinine

Due to the complex composition of serum and its many potential interference signals, the miniaturized Raman spectrometer (785 nm ID Raman, Ocean Optics, USA) used in the experiment

Biomedical Optics EXPRESS

has poor resolution (the highest resolution is only 4 cm^{-1}), which causes the characteristic creatinine peak to be easily obliterated. Therefore, we chose the confocal Raman microscope system (Horiba Jobin Yvon, HR Evolution, France) for the detection of serum creatinine. This instrument is equipped with a 633 nm He-Ne laser with a power of about 17 mW, a 50× objective lens of numerical aperture (NA) 0.5, a work distance (WD) of 10.6 mm, and a spectral resolution of 2 cm^{-1}. The filter and acquisition time were set at 10% and 3 s for measuring creatinine molecules to reduce the heating effect induced by the laser. According to the optical parameters of the confocal Raman instrument, we used COMSOL software to carry out a ray optical simulation, and the simulation result is shown in Figure S6. The simulation results showed that the SERS chip still had excellent Raman signal collection ability when using the confocal Raman instrument.

Figure 6(b) shows the SERS spectrum collected on the SERS chip after mixing normal human serum with different concentrations of creatinine (1×10^{-2} M to 1×10^{-5} M) in equal proportions. All spectra were deducted from the baseline by the asymmetric least squares smoothing method. Compared with the SERS spectrum of the creatinine aqueous solution, the Raman peak of serum was larger but the characteristic peak of creatinine at 678 cm^{-1} can be clearly distinguished. Furthermore, the intensity of the 678 cm^{-1} creatinine peak increased significantly in relation to increasing serum creatinine concentration. Using the added creatinine concentration as the abscissa and the peak at 678 cm^{-1} as the ordinate, a standard curve was established: $y = 963.63x+5053.17$ and $R2 = 0.91$, as shown in Fig. 6(c). The average value of the Raman intensity at 678 cm^{-1} of the SERS spectrum of normal human serum is about 239.29. When the serum creatinine concentration increased by 5 μM, the average peak value at 678 cm^{-1} increased to 321.14. This shows that the SERS chip can respond to changes in serum creatinine concentration of 5 μM, that is, the detection resolution is better than 5 μM.

3.3.3. Distinguishing between normal and patient serum

We performed SERS tests on serum samples from 40 different normal persons and 40 different renal dysfunction patients, and the results are shown in Figure S7a and 7b. Figure 6(d) shows the average SERS spectra of normal human serum and that of patients with renal dysfunction after normalization. It can be seen that, except for a certain difference in relative intensity, the main Raman peaks of the two sera are essentially the same. Furthermore, the value of the creatinine peak at 678 cm^{-1} is higher in serum from renal dysfunction patients than in normal human serum, indicating that the serum creatinine of these patients is higher than normal which is consistent with the clinical diagnosis results. The normalized SERS spectrum of patient serum at 678cm^{-1} had a peak range of 0.08~0.58, with an average value of 0.27, and the normal person's range of 0.02~0.18 and 0.09, respectively. As shown in Fig. 6(e), although the average peak value of the patients' serum at 678 cm^{-1} is higher than that of the normal population, the peak ranges partially overlap. We infer that this is mainly due to the interference by complex serum components. Thus, it is difficult to directly distinguish between the patients' and normal serum by the peak at 678 cm^{-1}.

We used principal component analysis to analyze the SERS spectra of sera from 40 normal people and 40 patients, extracting the principal components, and establishing recognition models. Figure 6(f) shows the spectral recognition model training set. The SERS spectra of 20 sera (10 normal and 10 patients) were used as blind samples, and discriminant analysis was used to identify them. The results are shown in Table S1. It can be seen from the table that all 10 normal persons were distinguished correctly, and two patients were judged to be normal. The overall detection accuracy rate was 90%.

4. Conclusions

In summary, we proposed a high-performance SERS chip with an integrated MOS and used it for rapid and accurate serum creatinine detection. The MOS optimizes the optical matching

Biomedical Optics EXPRESS

characteristics of the SERS substrate and the Raman detection system, and greatly improves the SERS detection sensitivity by improving the collection efficiency of the Raman scattering signal. The liquid-liquid interface self-assembly method was used to assemble single-layer silver nanoparticle arrays on Si wafers and Au-plated Si wafers as SERS active substrates. The study found that the AEF when using Au-plated Si wafers was about 5.6 times that of using Si wafers, with values of up to 3.51×10^7. The RSD calculated from the peaks of the R6G SERS spectrum at 612, 1509, and 1358 cm^{-1} were 10.7%, 11.2%, and 9.3%, respectively. Indicating an excellent signal uniformity. Then, we fabricated the micro-reflecting cavity based on a single-crystal Si wafer through a wet etching process, and then covered the micro-reflecting cavity with a micro-lens to form the MOS for increasing the collection efficiency of the scattered Raman signals. The experimental results show that the MOS can increase the Raman intensity more than four-fold and the AEF of the prepared SERS chip was as high as 1.46×10^8. We used the prepared SERS chip for creatinine detection experiments. The results showed that detection limits of creatinine in aqueous solution and serum of 1×10^{-6} M and 1×10^{-5} M, respectively, and we finding that the Raman intensity of serum at 678 cm^{-1} in the renal patients was generally higher than that in normal people, indicating that the serum creatinine concentrations of patients were greater than those of the normal population, which is consistent with the clinical diagnosis. In addition, we used the principal component analysis-linear discriminant method to distinguish sera normal people and patients, and the results showed that the corrected rate of blind sample identification reached 90%. This rapid detection method of serum creatinine based on the SERS chip provides a new option for the clinical diagnosis of kidney disease.

Funding. National Key Research and Development Program of China (2018YFB2002302); National Natural Science Foundation of China (61971074); research project of Sichuan University of Arts and Science (2019PT002Z); research project of Sichuan Provincial Key Lab of Process Equipment and Control (GK202002); Natural Science Foundation of Chongqing (cstc2019jcyj-xfkxX0003).

Acknowledgements. We would like to thank Mr. Deng Chao (Electron Microscopy Center of Chongqing University), Mr. Gong Xiangnan (Analysis and Test Center of Chongqing University) for their help in SEM and Raman characterization, respectively.

Disclosures. The authors declare no conflicts of interest.

Data availability. The data that support the findings of this study are available from the corresponding author upon reasonable request.

Supplemental document. See Supplement 1 for supporting content.

References

1. E. Owens, K. S. Tan, R. Ellis, S. Del Vecchio, T. Humphries, E. Lennan, D. Vesey, H. Healy, W. Hoy, and G. Gobe, "Development of a biomarker panel to distinguish risk of progressive chronic kidney disease," Biomedicines **8**(12), 606 (2020).
2. D. W. Cockcroft and M. H. Gault, "Prediction of creatinine clearance from serum creatinine," Nephron **16**(1), 31–41 (1976).
3. A. S. Levey, L. A. Stevens, C. H. Schmid, Y. P. Zhang, A. F. Castro, H. I. Feldman, J. W. Kusek, P. Eggers, F. Van Lente, T. Greene, and J. Coresh, and C. Chronic Kidney Dis Epidemiology, "A new equation to estimate glomerular filtration rate," Ann. Intern. Med. **150** (9), 604–612 (2009).
4. A. N. Zhu, X. Y. Zhao, M. Y. Cheng, L. Chen, Y. X. Wang, X. L. Zhang, Y. J. Zhang, and X. F. Zhang, "Nanohoneycomb surface-enhanced Raman spectroscopy-active chip for the determination of biomarkers of hepatocellular carcinoma," ACS Appl. Mater. Interfaces **11**(47), 44617–44623 (2019).
5. J. Wang, K. M. Koo, Y. L. Wang, and M. Trau, "Engineering state-of-the-art plasmonic nanomaterials for SERS-based clinical liquid biopsy applications," Adv. Sci. **6**(23), 1900730 (2019).
6. X. Zhao, J. Dong, E. Cao, Q. Y. Han, W. Gao, Y. K. Wang, J. X. Qi, and M. T. Sun, "Plasmon-exciton coupling by hybrids between graphene and gold nanorods vertical array for sensor," Appl. Mater. Today **14**, 166–174 (2019).
7. H. W. Qiu, M. Q. Wang, S. Z. Jiang, L. Zhang, Z. Yang, L. Li, J. J. Li, M. H. Cao, and J. Huang, "Reliable molecular trace-detection based on flexible SERS substrate of graphene/Ag-nanoflowers/PMMA," Sens. Actuators, B **249**, 439–450 (2017).
8. H. G. Lee, W. Choi, S. Y. Yang, D. H. Kim, S. G. Park, M. Y. Lee, and H. S. Jung, "PCR-coupled paper-based surface-enhanced Raman scattering (SERS) sensor for rapid and sensitive detection of respiratory bacterial DNA," Sens. Actuators, B **326**, 128802 (2021).

Biomedical Optics EXPRESS

9. Q. Z. Wang, Z. H. Xu, Y. J. Zhao, H. Zhangsun, T. Bu, C. Q. Zhang, X. Wang, and L. Wang, "Bio-inspired self-cleaning carbon cloth based on flower-like Ag nanoparticles and leaf-like MOF: a high-performance and reusable substrate for SERS detection of azo dyes in soft drinks," Sens. Actuators, B **329**, 129080 (2021).
10. R. S. Juang, Y. W. Cheng, W. T. Chen, K. S. Wang, C. C. Fu, S. H. Liu, R. J. Jeng, C. C. Chen, M. C. Yang, and T. Y. Liu, "Silver nanoparticles embedded on mesoporous-silica modified reduced graphene-oxide nanosheets for SERS detection of uremic toxins and parathyroid hormone," Appl. Surf. Sci. **521**, 146372 (2020).
11. W. I. K. Chio, S. Moorthy, J. Perumal, U. S. Dinish, I. P. Parkin, M. Olivo, and T. C. Lee, "Dual-triggered nanoaggregates of cucurbit 7 uril and gold nanoparticles for multi-spectroscopic quantification of creatinine in urinalysis," J. Mater. Chem. C **8**(21), 7051–7058 (2020).
12. W. Zhu, B. Y. Wen, L. J. Jie, X. D. Tian, Z. L. Yang, P. M. Radjenovic, S. Y. Luo, Z. Q. Tian, and J. F. Li, "Rapid and low-cost quantitative detection of creatinine in human urine with a portable Raman spectrometer," Biosens. Bioelectron. **154**, 112067 (2020).
13. D. Lin, C. L. Hsieh, K. C. Hsu, P. H. Liao, S. F. Qiu, T. X. Gong, K. T. Yong, S. Y. Feng, and K. V. Kong, "Geometrically encoded SERS nanobarcodes for the logical detection of nasopharyngeal carcinoma-related progression biomarkers," Nat. Commun. **12**(1), 16 (2021).
14. X. Su, Y. Xu, H. Z. Zhao, S. B. Li, and L. Chen, "Design and preparation of centrifugal microfluidic chip integrated with SERS detection for rapid diagnostics," Talanta **194**, 903–909 (2019).
15. K. Zhang, Y. Liu, Y. Wang, R. Zhang, J. Liu, J. Wei, H. Qian, K. Qian, R. Chen, and B. Liu, "Quantitative SERS detection of dopamine in cerebrospinal fluid by dual-recognition-induced hot spot generation," ACS Appl. Mater. Interfaces **10**(18), 15388–15394 (2018).
16. V. D. Phung, W. S. Jung, T. A. Nguyen, J. H. Kim, and S. W. Lee, "Reliable and quantitative SERS detection of dopamine levels in human blood plasma using a plasmonic Au/Ag nanocluster substrate," Nanoscale **10**(47), 22493–22503 (2018).
17. R. Stosch, A. Henrion, D. Schiel, and B. Guttler, "Surface enhanced Raman scattering based approach for quantitative determination of creatinine in human serum," Anal. Chem. **77**(22), 7386–7392 (2005).
18. J. F. Li, Y. J. Zhang, S. Y. Ding, R. Panneerselvam, and Z. Q. Tian, "Core-shell nanoparticle-enhanced Raman spectroscopy," Chem. Rev. **117**(7), 5002–5069 (2017).
19. S. Y. Ding, J. Yi, J. F. Li, B. Ren, D. Y. Wu, R. Panneerselvam, and Z. Q. Tian, "Nanostructure-based plasmon-enhanced Raman spectroscopy for surface analysis of materials," Nat. Rev. Mater. **1**(6), 16021 (2016).
20. J. M. Nam, J. W. Oh, H. Lee, and Y. D. Suh, "Plasmonic nanogap-enhanced Raman scattering with nanoparticles," Acc. Chem. Res. **49**(12), 2746–2755 (2016).
21. J. Dong, X. Zhao, E. Cao, Q. Y. Han, L. Liu, W. W. Zhang, W. Gao, J. Shi, Z. P. Zheng, D. D. Han, and M. T. Sun, "Flexible and transparent Au nanoparticle/graphene/Au nanoparticle 'sandwich' substrate for surface-enhanced Raman scattering," Mater. Today Nano **9**, 100067 (2020).
22. S. Y. Ding, E. M. You, Z. Q. Tian, and M. Moskovits, "Electromagnetic theories of surface-enhanced Raman spectroscopy," Chem. Soc. Rev. **46**(13), 4042–4076 (2017).
23. S. Kasani, K. Curtin, and N. Q. Wu, "A review of 2D and 3D plasmonic nanostructure array patterns: fabrication, light management and sensing applications," Nanophotonics **8**(12), 2065–2089 (2019).
24. T. H. Wu and Y. W. Lin, "Surface-enhanced Raman scattering active gold nanoparticle/nanohole arrays fabricated through electron beam lithography," Appl. Surf. Sci. **435**, 1143–1149 (2018).
25. M. M. P. Arnob, F. S. Zhao, J. T. Li, and W. C. Shih, "EBL-based fabrication and different modeling approaches for nanoporous gold nanodisks," ACS Photonics **4**(8), 1870–1878 (2017).
26. K. Sivashanmugan, J. D. Liao, J. W. You, and C. L. Wu, "Focused-ion-beam-fabricated Au/Ag multilayered nanorod array as SERS-active substrate for virus strain detection," Sens. Actuators, B **181**, 361–367 (2013).
27. M. K. Fan, G. F. S. Andrade, and A. G. Brolo, "A review on the fabrication of substrates for surface enhanced Raman spectroscopy and their applications in analytical chemistry," Anal. Chim. Acta **693**(1-2), 7–25 (2011).
28. T. Lee, S. Kwon, S. Jung, H. Lim, and J. J. Lee, "Macroscopic Ag nanostructure array patterns with high-density hotspots for reliable and ultra-sensitive SERS substrates," Nano Res. **12**(10), 2554–2558 (2019).
29. M. Cottat, N. Lidgi-Guigui, I. Tijunelyte, G. Barbillon, F. Hamouda, P. Gogol, A. Aassime, J. M. Lourtioz, B. Bartenlian, and M. de la Chapelle, "Soft UV nanoimprint lithography-designed highly sensitive substrates for SERS detection," Nanoscale Res. Lett. **9**(1), 623 (2014).
30. P. C. Lee and D. Meisel, "Adsorption and surface-enhanced Raman of dyes on silver and gold sols," J. Phys. Chem. **86**(17), 3391–3395 (1982).
31. G. Frens, "Controlled nucleation for regulation of particle-size in monodisperse gold suspensions," Nature (London), Phys. Sci. **241**(105), 20–22 (1973).
32. M. P. Konrad, A. P. Doherty, and S. E. Bell, "Stable and uniform SERS signals from self-assembled two-dimensional interfacial arrays of optically coupled Ag nanoparticles," Anal. Chem. **85**(14), 6783–6789 (2013).
33. M. P. Cecchini, V. A. Turek, J. Paget, A. A. Kornyshev, and J. B. Edel, "Self-assembled nanoparticle arrays for multiphase trace analyte detection," Nat. Mater. **12**(2), 165–171 (2013).
34. D. X. Wang, W. Q. Zhu, Y. Z. Chu, and K. B. Crozier, "High directivity optical antenna substrates for surface enhanced Raman scattering," Adv. Mater. **24**(32), 4376–4380 (2012).
35. Y. J. Gu, H. B. Li, S. P. Xu, Y. Liu, and W. Q. Xu, "Evanescent field excited plasmonic nano-antenna for improving SERS signal," Phys. Chem. Chem. Phys. **15**(37), 15494–15498 (2013).

Biomedical Optics EXPRESS

36. H. L. Wang, Y. Y. Wang, Y. Wang, W. Q. Xu, and S. P. Xu, "Modulation of hot regions in waveguide-based evanescent-field-coupled localized surface plasmons for plasmon-enhanced spectroscopy," Photonics Res. **5**(5), 527–535 (2017).
37. H. L. Wang, H. B. Li, S. P. Xu, B. Zhao, and W. Q. Xu, "Integrated plasmon-enhanced Raman scattering (iPERS) spectroscopy," Sci. Rep. **7**(1), 14630 (2017).
38. F. Yang, P. Wen, Z. Q. Zhang, D. Y. Li, L. Chen, and S. B. Li, "High signal collection efficiency in a 3D SERS chip using a micro-reflector," Opt. Express **28**(26), 39790–39798 (2020).
39. S.-Y. Ding, J. Yi, J.-F. Li, and Z.-Q. Tian, "A theoretical and experimental approach to shell-isolated nanoparticle-enhanced Raman spectroscopy of single-crystal electrodes," Surf. Sci. **631**, 73–80 (2015).
40. K. Vikram, S. Mishra, S. K. Srivastava, and R. K. Singh, "Low temperature Raman and DFT study of creatinine," J. Mol. Struct. **1012**, 141–150 (2012).